

Deformation induced crystallization and associated morphology development of carbon nanotube - PVDF nanocomposites

Gaurav Mago¹, Frank T. Fisher¹ and Dilhan M. Kalyon^{2,*}

¹Department of Mechanical Engineering
Stevens Institute of Technology
Hoboken, NJ 07030, USA
Email address: Frank.Fisher@stevens.edu

²Chemical, Biomedical and Materials Engineering Department
Stevens Institute of Technology
Hoboken, NJ 07030, USA
Email address: Dilhan.Kalyon@stevens.edu

ABSTRACT

Poly(vinylidene fluoride) (PVDF) is a semi-crystalline thermoplastic polymer that is of interest for sensor, actuator and biomedical applications because of its piezoelectric and pyroelectric properties, as well as outstanding mechanical and chemical properties. Although it is known that the shear-induced crystallization behavior of nanocomposites can be significantly affected by the presence of nanoparticles, the effects of the incorporation of carbon nanotubes on the deformation-induced crystallization and associated morphology development of PVDF have not been previously investigated. Here the dynamics of the shear induced crystallization of carbon nanotubes incorporated in PVDF were investigated using simple shear flow. The shear-induced crystallization behavior was affected by the deformation rate, temperature, and the concentration of the carbon nanotubes. Time-dependence of linear viscoelastic properties indicated that the presence of multi-walled carbon nanotubes (MWNTs) in PVDF greatly altered the shear-induced crystallization kinetics of PVDF, while no significant changes in crystallization behavior were observed for pure PVDF samples sheared under similar conditions. Upon increase of the concentration of the MWNTs the crystal size of PVDF decreased while its rate of crystallization increased in conjunction with an increase of the β phase crystallization. Overall, these findings suggest that the shear-induced crystallization of PVDF nanocomposites (and in general flow-induced crystallization effects associated with the thermo-mechanical history experienced by the nanocomposite during processing) should be integral parts of attempts to generate a comprehensive understanding of the development of the microstructural distributions and the coupled ultimate properties of polymer nanocomposites.

Keywords: Poly (vinylidene fluoride), nanocomposite, crystal phase, shear-induced crystallization, rheology

1. INTRODUCTION

Polyvinylidene fluoride (PVDF) is a semicrystalline thermoplastic polymer which is used widely for various device applications, including sensors and actuators, due to its promising piezoelectric and pyroelectric properties, which are governed by its crystalline structure. There are five known polymorphs of PVDF, such as α , β , γ , δ and ϵ .¹⁻³ The α -phase is most common upon crystallization from the melt and is the dominant crystalline phase, while the β form exhibits the most piezoelectric, pyroelectric and ferroelectric activities; it is this latter form that endues PVDF with great potential for various device applications such as sensors and transducers.⁴ It is for this reason that various processing methods have been pursued to yield this β form crystal structure in PVDF. For example, crystallization in the β -phase can be achieved by melt crystallization under high pressure, by application of strong electric field, by uniaxial stretching during crystallization, or by crystallization from solution.⁵⁻¹⁰ The β form can also be formed upon melt-spinning and drawing of PVDF.¹¹ During melt spinning the β phase was found to increase with the spinline normal stress difference, while the quiescently crystallized PVDF exhibited the α -crystalline form. Schultz et al¹² studied the mechanisms of microstructure development upon crystallization from melt-spinning of PVDF, using *in-situ* X-ray techniques and documented the formation of shish-kebab type crystals. Such extensional flow based processing techniques significantly affect the polymer crystal structure due to the preferred orientation of the macromolecules prior to crystallization and thus lead to the improvement of the mechanical properties.^{6, 13-15} Further, the incorporation of nanoparticles can also affect the crystal structure of polymers. Shah et al found that melt compounding of nanoclays into PVDF increases the toughness and β -phase formation in the nanocomposite.^{16, 17} The β -phase can also be increased by the presence of carbon nanotubes.¹⁸ The compounding of nanoparticles into PVDF is especially attractive because of the significant increase in the electromechanical coefficient to enable the use of the resulting nanocomposites as actuators for artificial muscles and sensors for vibration control, along with improvements in the mechanical properties.¹⁹⁻²²

The physical properties of semi-crystalline polymers depend upon the processing conditions and can also be strongly influenced by the presence of nanoparticles, which affect the crystallization behavior and the resulting crystal morphology developed within the processed sample.²³⁻²⁶ Industrial polymer processing methods involve very complex deformation histories, which may affect the nucleation and crystallization behavior of polymers and their nanocomposites.^{11, 13, 15, 27-32} For example, it is known that the application of a shear stress to a polymer melt at temperatures which are in the vicinity of the crystallization temperature of the polymer (at which crystallization would not have occurred under quiescent conditions) leads to the preferred orientation of the macromolecules, thus reducing the entropy of the melt and leading to

the flow-induced crystallization from the melt.²⁴ Furthermore, the presence of nanoparticles alters the dynamics of shear induced crystallization from the melt. For example, it has been found that the incorporation of multi-walled carbon nanotubes (MWNTs) promote the shear-induced crystallization behavior and the developed morphology of poly (butylene terephthalate) (PBT) nanocomposites.³³ Thus, a detailed understanding of the roles played by the nucleation and crystallization processes under shear is necessary to optimize the processing of the nanocomposites and to tailor their various ultimate properties. Although various studies have been carried out to understand the effect of processing conditions on crystal structure and morphology of PVDF, to our knowledge there are no studies focusing on the influence of the processing conditions on the development of the PVDF crystalline forms in the presence of nanoparticles. The goal of this study is: (1) to study the shear-induced crystallization behavior of MWNT-PVDF nanocomposites using the time and the deformation rate dependence of the linear viscoelastic properties as the principal tool and (2) to document the effects of the presence and concentration of the MWNTs on crystallization behavior of MWNT-PVDF nanocomposites and on the development of the microstructural distributions (and β -crystal formation) in articles processed from MWNT-PVDF nanocomposites.

2. EXPERIMENTAL

Materials

Powdered PVDF (Kynar 741) was obtained from Arkema Inc (USA). As reported by the manufacturer, its weight average molecular weight is 250,000 and its density is 1.78 g/cm³. The MWNTs (trade name: MWNT-A-P) were purchased from Sunnano (China). As reported by the manufacturer, the diameter of the MWNTs was 10-30 nm, and the average bulk density was 1.5 g/cm³. To examine the size and shape distributions of the MWNTs a LEO 1550 scanning electron microscope (SEM), operated at 5kV, was used. Figure 1 shows a typical scanning electron micrograph of the as-received MWNTs used in this work.

Melt processing of MWNT-PVDF nanocomposites

There are several ways of dispersing nanofillers into polymers including solution mixing, in-situ polymerization, and melt compounding. In many potential applications melt compounding is the generally preferred method due to its relatively low cost, high productivity, and its compatibility with other conventional polymer processing techniques. Here MWNT-PVDF nanocomposites were melt compounded in a Haake torque rheometer with a 300 ml intensive

mixing head. The torque rheometer is an intensive mixer (a mini-Banbury mixer) with the capability of measuring torque and hence specific energy input during the mixing process under isothermal conditions. Mixing of MWNTs with PVDF was carried at 220°C for 10 minutes at 50 rpm. The loading levels of the nanocomposites were 0.01, 0.1, 0.5, 1, 2 and 5.0% (by volume) of MWNTs. After mixing the nanocomposite was removed and sealed within two polyethylene bags. These specimens were compression molded using a Carver hot press at 220°C for 5 minutes, followed by the characterization of linear viscoelastic material functions of the nanocomposite samples. Pure PVDF was processed and characterized under identical conditions as a control.

Characterization of linear viscoelastic properties

The linear viscoelastic material functions of PVDF and MWNT-PVDF nanocomposites were characterized by employing small-amplitude oscillatory shear using an ARES (Advanced Rheometric Expansion System) with a force rebalance transducer (2K-FRTN1) available from TA Instruments. The actuator of the ARES is a *dc* servomotor with a shaft supported by an air bearing with an angular displacement range of 0.05-500 mrad. Oven temperature is controlled within $\pm 0.1^\circ\text{C}$. The test fixtures consisted of 25 mm diameter stainless steel parallel plates. Frequency sweeps between 0.01 and 100 rad/s were carried out at 1% strain, which was determined to be within the linear viscoelastic range for all of the samples tested. For the isothermal crystallization study under shear, the samples were molten at 200°C and the final gap was set to 0.7 mm, after which the excess specimen protruding out of the gap was carefully trimmed using a razor blade. Upon loading and temperature equilibration, the specimen was allowed to relax for 5 minutes, after which it was cooled to the targeted test temperature for the characterization of the dynamic properties as a function of the strain amplitude, frequency and time.

Thermal Analysis and WAXD analysis

Differential Scanning Calorimetry (DSC) studies were conducted using a TA Instruments (New Castle, DE) DSC model Q1000 on pure PVDF and PVDF nanocomposites. The DSC samples were ramped from 25 to 200°C, and maintained under isothermal conditions for 5 minutes at 25 and 200°C. The specimens were heated and cooled at a rate of 10°C/min. The relative degree of crystallinity was determined as the ratio of the integrated heat of fusion of the sample, determined during the heating of the sample to 200°C, to the heat of fusion of purely crystalline PVDF. Wide angle X-ray diffraction (WAXD) data were collected at room temperature by positioning the sample on a quartz sample holder using a Rigaku Miniflex diffractometer in

conjunction with a CuK_α radiation source ($\lambda = 0.154 \text{ nm}$) operated at 30kV. The x-ray diffractograms were collected in the scan range 2θ of $10\text{-}50^\circ$ at the scan speed of 1° min^{-1} and using a step size of 0.04° .

3. RESULTS AND DISCUSSION

Linear viscoelastic material functions (storage moduli, loss moduli, magnitude of complex viscosity) are very sensitive to structural changes in the molten polymer and can provide information on the change in the physicochemical properties of the polymer during deformation. For example, for thermally sensitive polymer melts, an irreversible decrease in viscosity with time at a constant shear rate suggests the possibility of molecular weight break-down, whereas an irreversible increase in viscosity with time can suggest the possibility of chemical cross-linking. Both thermal degradation and chemical cross-linking are irreversible. On the other hand, a reversible change in the linear viscoelastic properties with time during shearing under constant frequency, temperature and strain amplitude can indicate the flow-induced crystallization of the polymer melt occurring at a temperature which is greater than the crystallization temperature of the pure melt.^{24, 34, 35} During the time sweep experiment unbounded monotonic increases in the storage moduli (G'), magnitude of complex viscosity $|\eta^*|$, and loss moduli (G'') with time thus suggest the onset of crystallization induced by the applied shear. Pennings and co-workers have documented that the morphology of such crystals is typically of the “shish kebab” type and is thus very different than the spherulitic morphologies that are generally observed under quiescent crystallization conditions.³⁶⁻³⁸

Figure 2 shows the the storage modulus (G') of PVDF and PVDF nanocomposites at 190°C at 1% strain amplitude and 1 rps as a function of time. The behavior is steady suggesting that the PVDF melt and its suspensions are stable at 190°C . In Figure 3, the presence of MWNTs give rise to modest increases in the storage modulus, the magnitude of complex viscosity, and loss modulus values over the 0.01 to 100 rps frequency range. When the concentration of the MWNTs are $\geq 2\%$ by volume the loss modulus G'' is greater than the storage modulus G' in the low frequency range of 0.01-1.6 rps. As the frequency increases the storage modulus values increase at a greater rate in comparison to the loss modulus values and a cross-over occurs at around 2 rps. Approaches to the Newtonian behavior are observed at the low frequency range for all concentrations of MWNTs (Fig. (3(b))). The incorporation of MWNTs modestly increases the magnitude of complex viscosity of the PVDF nanocomposites with the increase most pronounced at a concentration of the highest MWNT concentration of 5% by volume. The G' , $|\eta^*|$ and G'' curves are all parallel to each other, regardless of the concentration of the MWNTs in the 0.01 to 5% range (Figure 3) suggesting that

the incorporation of the nanotubes has not significantly altered the microstructure of the suspensions and only modest increases in the relaxation times have occurred (akin to the thermo-rheological simplicity associated with changes in temperature).

Figure 4 shows the time dependent behavior of storage modulus, G' , of unfilled PVDF in the range of 150 to 190°C. In these experiments the strain amplitude and the frequency are kept constant at 1% and 1 rps, respectively. It is observed that the storage modulus remains constant with shearing time in the 158-190°C range. However, at the lower temperatures of 150 and 152°C, a rapid increase of the storage modulus occurs as a function of time as a result of shear-induced crystallization of the polymer melt. Similar results have been observed by others on poly (ϵ -lactone),³⁹ polyethylene,^{24,34} and poly(ethylene terephthalate)⁴⁰ melts.

The work of de Gennes in dilute solutions of polymers has revealed that during flow the polymer chains undergo a step change from a random coil to a fully extended chain conformation at a critical strain rate, without any intermediate stable chain conformations.⁴¹ The subsequent studies of Keller et al¹³ have provided experimental evidence of the coil-stretch transition in polymer crystallization under shear and extension, demonstrating that as the strain rate is increased during deformation there is an abrupt change in birefringence indicative of the formation of a fully-extended chain conformation at the critical strain rate. Such extension and orientation of the macromolecules in the flow direction reduce the energy barrier necessary to be overcome for nuclei to form, and thus lead to the crystallization of the polymer at temperatures under which quiescent crystallization would not have occurred. Shear induced crystallization of the PVDF clearly occurs at a higher rate with decreasing temperature (Figure 4). What are the effects of the carbon nanotubes on the shear induced crystallization behavior of PVDF?

Effect of MWNT loading on PVDF crystallization behavior under shear

Figure 5 shows the time dependence of the G' , G'' , $|\eta^*|$ and the loss tangent ($\tan \delta = G''/G'$) data for PVDF and PVDF nanocomposites for a constant frequency of 1 rps and 1% strain amplitude at 158°C. As shown in Figure 5(a), increases in the storage modulus, G' , values with increasing time were observed for the PVDF nanocomposites that were not observed for pure PVDF under similar conditions. The increase in the storage moduli with time is indicative of the shear-induced crystallization of PVDF as affected by the presence and the concentration of MWNTs. The storage modulus values increase up to the point that the force balance transducer of the rheometer is overloaded (the torque reaches over 2,000 N-m). Furthermore, an increase in the concentration of MWNTs shows a decrease of the induction time for the onset of crystallization. Here the induction times for crystallization are in the range of 2800-1500s for 0.5-5% MWNTs by

volume. The most likely mechanism for the onset of the crystallization of the MWNT incorporated suspensions at a temperature of 158°C is that the nanoparticles act as heterogeneous nucleating agents. During heterogeneous nucleation the rate of nucleation is principally controlled by the concentration of the heterogeneous nuclei. The decrease of the induction time for crystallization with increased concentration of nanotubes may be associated with an increase of the nucleation rate with increasing concentration. A decrease in the induction time for crystallization under quiescent conditions has been reported and was associated with the presence of nanoparticles.^{30, 42-44} Shear induced crystallization behavior of nanocomposites associated with the presence of nanotubes has also been observed during isothermal crystallization under shear studies of PBT nanocomposites.³³

The concomitant increases of the other dynamic properties, i.e., the loss modulus (Fig. 5(b)) and the magnitude of complex viscosity (Fig. 5(c)) with shearing time are also shown in Figure 5. Similar to the behavior of the storage modulus, the loss modulus and the magnitude of complex viscosity values also exhibit increases with shearing time, with the rate of increase greater for greater concentration of MWNTs. The formation of the crystals should lead to increases in the affine junction points in the entangled melt to render relaxation more difficult, thus increasing both the elasticity and the viscosity of the melt. The magnitude of complex viscosity values of PVDF nanocomposites are orders of magnitude higher than those of the pure PVDF, indicating the introduction of a significant degree of crystallinity as induced by the presence of the MWNTs. Figure 5(d) shows a decrease of tan delta with time, with the addition of MWNTs greatly reducing the loss tangent as affected by the more significant increases in the elasticity (as represented by the storage modulus, G') in comparison to the increase of the viscous energy dissipation (as represented by the loss modulus G'') with increasing shearing time.

The typical effect of temperature on the shear-induced crystallization behavior can be further seen through the set of small-amplitude oscillatory shear experiments carried out at the lower temperature of 152°C as shown in Figure 6. The increases of the storage modulus, loss modulus and the magnitude of complex viscosity with time associated with the presence of the nanotubes are more pronounced at the lower temperature. Furthermore, unlike the behavior at 158°C, at the lower temperature of 152°C the PVDF itself exhibits shear-induced crystallization, albeit at a much slower rate in comparison to the nanocomposites incorporated with 0.1-5% MWNTs. Similar to the results obtained at the higher temperature, the rate of crystallization was found to increase with the increase of the MWNT concentration. For MWNT loadings above 2% by volume, the rate of crystallization is relatively rapid (with induction time almost instantaneous with the torque reaching the overload limit of the transducer within 200s upon the initiation of shearing). The time dependent data for the 2%MWNT-PVDF cannot be distinguished from the data of 5% MWNT-PVDF nanocomposite due to instrument limitations.

It is interesting to note that shaping of PVDF and PVDF nanocomposites within the constraints of a typical polymer processing method (such as injection molding) involves rapid cooling in conjunction with different time scales for crystallization due to the significant differences in thermal and stress/pressure histories of the PVDF located at different locations in the cavity. Thus, it is anticipated that crystallization from the melt in a typical polymer processing operation will generate a wide range of stress induced crystallization conditions and give rise to myriad morphologies associated with such differences in the thermal, shearing and resulting crystallization histories.

Effect of deformation rate on crystallization behavior

Figure 7 shows the variation of G' , G'' , $|\eta^*|$ and $\tan \delta$ for 5%MWNT-PVDF nanocomposite with time at 158°C and at 1% strain amplitude for frequencies of 1, 3 and 5 rps. For pure PVDF no time-dependence was observed in the 1-5 rps range (i.e. there is no shear-induced crystallization of the pure PVDF under these conditions; data not shown). For the 5%MWNT-PVDF suspension all three frequencies gave rise to shear-induced crystallization, with the induction time for crystallization decreasing with increasing frequency. Similar frequency dependence was observed for PBT nanocomposites under shear.³³ Figure 7(d) shows a fast decrease in $\tan \delta$ with increasing frequency, due to an increase in crystallization rate which increases the storage modulus of the melt at a greater rate in comparison to the rate of increase of the loss modulus. This again emphasizes the greater role played by the elasticity in comparison to viscous dissipation with increasing degree of crystallinity, consistent with the results discussed earlier.

WAXD analysis of quiescent and sheared PVDF and PVDF nanocomposite samples

Figure 8 shows the WAXD spectra of PVDF and PVDF nanocomposite samples prepared under quiescent (compression molded) conditions. The pure PVDF sample is predominantly α -phase with characteristic peaks at 2θ values of 18.6°, 20.3° and 27.5°. ⁴⁵ With addition of MWNTs a change in relative intensity of peaks can be clearly seen. The increase in MWNTs loading decreases the peak at 18.6°, relative to the peak at 20.3°. Furthermore, the introduction of MWNTs produces a shoulder at 20.7°, which occupies a greater area with increasing MWNT loading. This peak at 20.7° does not overlap with the peaks associated with MWNTs (major peaks in the WAXD spectrum for MWNTs occur at 28.5°, 39.5° and 40.6°). Overall, the increases of the areas under the peaks associated with the Bragg angles of 20.3° and 20.7° are attributed to the formation of the β -phase crystal in PVDF nanocomposite samples while the decrease of the areas of the peaks at 20.3°

and 27.5° are attributed to the decrease of the α phase (the decrease in the 27.5° peak occurs in spite of the increase of the concentration of MWNTs). Similar results for the quiescent crystallization condition have been obtained upon melt-blending of PVDF with MWNTs and nanoclays.^{18, 20, 23}

Figure 9 shows the WAXD results of the 5%MWNT-PVDF nanocomposite sample collected after shearing at different frequencies at 158°C . The results were compared with 5%MWNT-PVDF nanocomposite sample crystallized under quiescent conditions in the ARES for 3000 s (i.e. with no shearing). In the sheared samples, the shoulder located at 20.7° attributed to the β -phase can be seen, as well as there is an increase in overall area under the peak. Such changes in crystallinity due to shearing versus the quiescent conditions should be tractable upon DSC analysis as will be shown below. Other studies have also revealed the generation of the β -phase upon deformation of the PVDF melt.¹¹ However, these earlier studies were carried out using fiber spinning, with the associated strong extensional flow, where the rate of separation between two initially adjacent points changes exponentially with respect to time, whereas the distance changes only linearly in the simple shear flow, as used in this study.

Thermal analysis of quiescent and sheared PVDF and PVDF nanocomposite samples

Typical differential scanning calorimetry (DSC) results depicting the melting and crystallization behavior of PVDF under non-equilibrium conditions are shown in Figure 10. Upon heating at the rate of $10^\circ\text{C}/\text{min}$, the melting onset is around 145°C , with a nominal melting temperature ($T_{m,p}$; the temperature of the peak of the melting endotherm upon heating) of 172.3°C and a melting temperature (T_m ; the highest temperature at which the last trace of crystallinity disappears) of 182.3°C . As shown in Table 1, the incorporation of the MWNTs followed by quiescent crystallization appears to result in a slight decrease of the mean value of the nominal melting temperature in comparison to the pure PVDF, with the decrease of the mean value of the nominal melting temperature being more pronounced with increasing concentration of the MWNTs. The mean values of the integrated heat of fusion values, ΔH_m , of the PVDF (corrected for the presence of carbon nanotubes, i.e., heat of fusion of the nanocomposite sample over the weight fraction of polymer in the sample) suggest that the degree of crystallinity overall appears to increase with increasing concentration of the MWNTs. The relative degree of crystallinity was determined as the ratio of the integrated heat of fusion of the sample, determined during the heating of the sample to 200°C , over the heat of fusion of purely crystalline PVDF (104.6 J/g).⁴⁶ As shown in Table 1, the mean values of the degree of crystallinity increases from 26.8% of the PVDF to over 30.5% upon the incorporation of MWNTs). However, it should be noted that Table 1 reports the

95% confidence intervals (based on five samples for each run) determined according to Student's-t distribution, and there is some overlap between the confidence intervals of the thermal properties of different nanocomposite samples. Such overlapping prevent the drawing of definite conclusions.

Figure 10(b) shows the crystallization behavior of pure PVDF after being kept at a isothermal temperature of 200°C for a duration of 5 minutes, and then cooling at a rate of 10°C/min. As shown in Table 1, the nominal crystallization temperature ($T_{c,p}$) values increase upon the incorporation of the MWNTs, consistent with the findings of other studies which have focused on the effect of nanotubes on quiescent crystallization behavior of Nylon-6⁴⁷ and polypropylene.^{44, 48} The relative shift of $T_{c,p}$ is even evident at the lowest concentration of MWNTs (with the mean T_c value increasing from 129.7 to 137.2°C upon the incorporation of only 0.01% of MWNTs). Such a spectacular rise is only possible due to the very high surface to volume ratio of the nanotubes as they act as heterogeneous nuclei. As typically reported in the literature, subsequent increases in the crystallization nominal temperature upon further increases in MWNT loading are less pronounced.

Table 2 shows the effect of MWNTs on the final crystallinity of 5%MWNT-PVDF nanocomposite samples collected after shearing in small-amplitude oscillatory shear at different frequencies followed by cooling to ambient under free convection (around 50-60°C/min). For comparison, the heat of fusion and degree of crystallinity values of 5%MWNT-PVDF nanocomposite sample, which was only thermally treated and kept in the confines of the rheometer for a duration of 3000 s, without actually being sheared, are also included. The mean values of the degree of crystallinity obtained at the constant loading level of 5% by volume of MWNTs suggest that the degree of crystallinity of the 5%MWNT-PVDF nanocomposite increases upon shearing. An increase in crystallinity upon shearing has been observed for other polymers including polypropylene and polyethylene blends.⁴⁹⁻⁵¹ The sheared samples have similar values of degree of crystallinity, irrespective of the frequency applied within the narrow range of 1-5 rps. The changes in the melting temperature are negligible.

Effect of MWNTs on PVDF crystal size

Figure 11 shows the effect of the incorporation of the MWNTs on PVDF spherulite sizes (as revealed by the Maltese cross patterns under the polarized light). Melt-mixed PVDF nanocomposite samples with 0.01 and 0.1% of MWNT loadings were subjected to the same analysis undertaken for virgin PVDF. The samples were molten and isothermally crystallized between two glass slides at 160 °C for 2h. The PVDF spherulite size decreased with addition of MWNTs. This is again consistent with the MWNTs acting as heterogeneous nuclei, with the

number of nuclei eventually defining the total number of spherulites upon the growth of the spherulites ceasing when the spherulites impinge on each other.

4. CONCLUSIONS

The effect of MWNTs on the time-dependent linear viscoelastic material functions, associated with shear-induced crystallization behavior and the resulting crystalline structures of PVDF nanocomposites, have been studied. The rate of PVDF crystallization under shear was increased due to the presence of MWNTs. The crystallization temperature was found to increase due to the heterogeneous nucleation effect of nanotubes, concomitant with the decrease of the PVDF crystal size. The addition of MWNTs and shearing appear to promote the formation of β -crystals in PVDF nanocomposites. These results suggest that the structure and morphology of PVDF nanocomposites will depend very strongly on the processing conditions, as well as on the concentrations of the nanotubes.

5. ACKNOWLEDGEMENTS

Financial support from the Department of Mechanical Engineering at Stevens (for GM) is greatly appreciated. The authors would like to thank Dr. Halil Gevgilili from the Highly Filled Materials Institute (HfMI) at Stevens for his contributions to this work. Arkema Inc (USA) is acknowledged for providing Kynar 741 PVDF powder.

6. REFERENCES

1. A. J. Lovinger, *Science* 220, 1115 (1983).
2. A. Ambrosy, K. Holdik, *J. Phys. E: Sci. Inst.* 17, 856 (1984).
3. T. Mirfakhrai, J. D. W. Madden, R. H. Baughman, *Materials Today* 10, 30 (2007).
4. M. G. Broadhurst, G. T. Davis, *Ferroelectrics* 60, 3 (1984).
5. G. T. Davis, J. E. McKinney, M. G. Broadhurst, S. C. Roth, *J. Appl. Phys.* 49, 4998 (1978).
6. J. Humphreys, I. M. Ward, T. McGrath, *J. Appl. Polym. Sci.* 30, 4069 (1985).
7. J. Scheinbeim, C. Nakafuku, B. A. Newman, K. D. Pae, *J. Appl. Phys.* 50, 4399 (1979).
8. R. Gregorio, E. M. Ueno, *J. Mater. Sci.* 34, 4489 (1999).
9. A. J. Lovinger, *Polymer* 22, 412 (1981).
10. K. Matsushige, T. Takemura, *J. Polym. Sci. :Part B: Polym. Phys.* 16, 921 (1978).
11. Y. Wang, M. Cakmak, J. L. White, *J. Appl. Polym. Sci.* 30, 2615 (1985).
12. J. M. Schultz, B. S. Hsiao, J. M. Samon, *Polymer* 41, 8887 (2000).
13. A. Keller, H. Kolnaar, *Processing of polymers*. H. E. H. Meijer, Ed., Material Science and Technology, Processing of Polymers (Materials Science and Technology: A Comprehensive Treatment) (Wiley-VCH, New York, July, 1997), pp. 189.
14. D. M. Bigg, *Polym. Eng. Sci.* 28, 830 (1988).
15. A. Keller, M. J. Machin, *J. Macromol. Sci.: Phys.* B1, 41 (1967).
16. D. Shah, P. Maiti, E. Gunn, D. F. Schmidt, D. D. Jiang, C. A. Batt, E. P. Giannelis, *Adv. Mater.* 16, 1173 (2004).

17. D. Shah, P. Maiti, D. D. Jiang, C. A. Batt, E. A. Giannelis, *Adv. Mater.* 17, 525 (2005).
18. Y. W. Nam, W. N. Kim, Y. H. Cho, D. W. Chae, G. H. Kim, S. P. Hong, S. S. Hwang, S. M. Hong, *Macromol. Symp.* 249-250, 478 (2007).
19. Z. Dang, Y. Lin, C. Nan, *Adv. Mater.* 15, 1625 (2003).
20. N. Levi, R. Czerw, S. Xing, P. Iyer, D. L. Carroll, *Nano Lett.* 4, 1267 (2004).
21. A. Ramaratnam, N. Jalili, *J. Intell. Mater. Syst. Struct.* 17, 199 (2006).
22. A. Ramaratnam, N. Jalili, H. Rajoria, *Proc. SPIE* 5503, 478 (2004).
23. D. R. Dillon, K. K. Tenneti, C. Y. Li, F. K. Ko, I. Sics, B. S. Hsiao, *Polymer* 47, 1678 (2006).
24. M. Kamal, D. M. Kalyon, J. Dealy, *Polym. Eng. Sci.* 20, 1117 (1980).
25. L. Priya, J. P. Jog, *J. Appl. Polym. Sci.* 89, 2036 (2003).
26. H. Sobhani, M. Razavi-Nouri, A. A. Yousefi, *J. Appl. Polym. Sci.* 104, 89 (2007).
27. J. M. Samon, J. M. Schultz, B. S. Hsiao, S. Seifert, N. Striebeck, I. Gurke, G. Collins, C. Saw, *Macromolecules* 32, 8121 (1999).
28. J. N. Ness, J. Z. Liang, *J. Appl. Polym. Sci.* 48, 557 (1993).
29. M. R. Mackley, F. C. Frank, A. Keller, *J. Mater. Sci.* 10, 1501 (1975).
30. W. Leelapornpisit, M. Ton-That, F. Perrin-Sarazin, K. Cole, J. Denault, B. Simard, *J. Polym. Sci. :Part B: Polym. Phys.* 43, 2445 (2005).
31. A. G. Kolbeck, D. R. Uhlmann, *J. Polym. Sci. :Part B: Polym. Phys.* 15, 27 (1977).
32. A. J. McHugh, *J. Appl. Polym. Sci.* 19, 125 (1975).
33. G. Mago, F. T. Fisher, D. M. Kalyon, *Proc. ASME Int. Mech. Eng. Conf. Expo. (IMECE), Chicago, IL (November 5-10, 2006)*.
34. C. Carrot, J. Guillet, K. Boutahar, *Rheol. Acta* 32, 566 (1993).
35. K. Boutahar, C. Carrot, J. Guillet, *Macromolecules* 31, 1921 (1998).
36. A. Zwijnenburg, A. J. Pennings, *Colloid. Polym. Sci.* 253, 452 (1975).
37. A. Zwijnenburg, A. J. Pennings, *Colloid. Polym. Sci.* 254, 868 (1976).
38. A. J. Pennings, *J. Cryst. Growth* 48, 574 (1980).
39. C. H. Sherwood, F. P. Price, R. S. Stein, *J. Polym. Sci.: Polym. Symp.* 63, 77 (1978).
40. H. S. Myung, M. J. Yoon, E. S. Yoo, B. C. Kim, S. S. Im, *J. Appl. Polym. Sci.* 80, 2640 (2001).
41. P. G. de Gennes, *J. Chem. Phys.* 60, 5030 (1974).
42. J. Sandler, G. Broza, M. Nolte, K. Schulte, Y. M. Lam, M. S. P. Shaffer, *J. Macromol. Sci.: Phys.* B42, 479 (2003).
43. E. Assouline, A. Lustiger, A. H. Barber, C. A. Cooper, E. Klein, E. Wachtel, H. D. Wagner, *J. Polym. Sci. :Part B: Polym. Phys.* 41, 520 (2003).
44. B. P. Grady, F. Pompeo, R. L. Shambaugh, D. E. Resasco, *J. Phys. Chem. B* 106, 5852 (2002).
45. M. G. Buonomenna, P. Macchi, M. Davoli, E. Drioli, *Eur. Polym. J.* 43, 1557 (2007).
46. J. Buckley, P. Cebe, D. Cherdack, J. Crawford, B. S. Ince, M. Jenkins, J. Pan, M. Reveley, N. Washington, N. Wolchover, *Polymer* 47, 2411 (2006).
47. D. Chae, S. Oh, B. C. Kim, *J. Polym. Sci. :Part B: Polym. Phys.* 42, 790 (2004).
48. A. R. Bhattacharya, T. V. Sreekumar, T. Liu, S. Kumar, L. Ericson, R. Hauge, R. E. Smalley, *Polymer* 44, 2373 (2003).
49. L. Yang, R. H. Somani, I. Sics, B. S. Hsiao, R. Kolb, H. Fruitwala, C. Ong, *Macromolecules* 37, 4845 (2004).
50. A. Nogales, B. S. Hsiao, R. H. Somani, S. Srinivas, A. H. Tsou, F. J. Balta-calleja, T. A. Ezquerro, *Polymer* 42, 5247 (2001).
51. B. S. Hsiao, L. Yang, R. H. Somani, C. A. Avila-Orta, L. Zhu, *Phys. Rev. Lett.* 94, 117802 (2005).

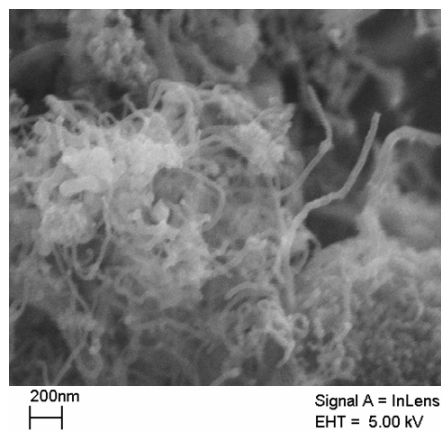


Figure 1: SEM image of the as-received MWNTs used in this work

Deformation induced crystallization and associated morphology development of carbon nanotube-PVDF nanocomposites, Mago, Fisher and Kalyon

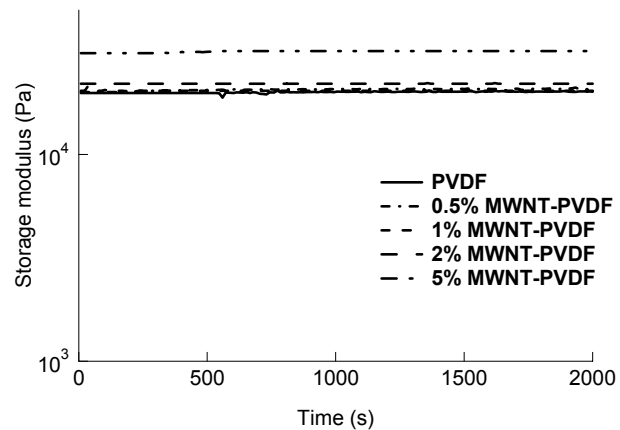


Figure 2: Change in storage modulus (G') of PVDF and PVDF nanocomposites at 190°C (1% strain, 1 rps)

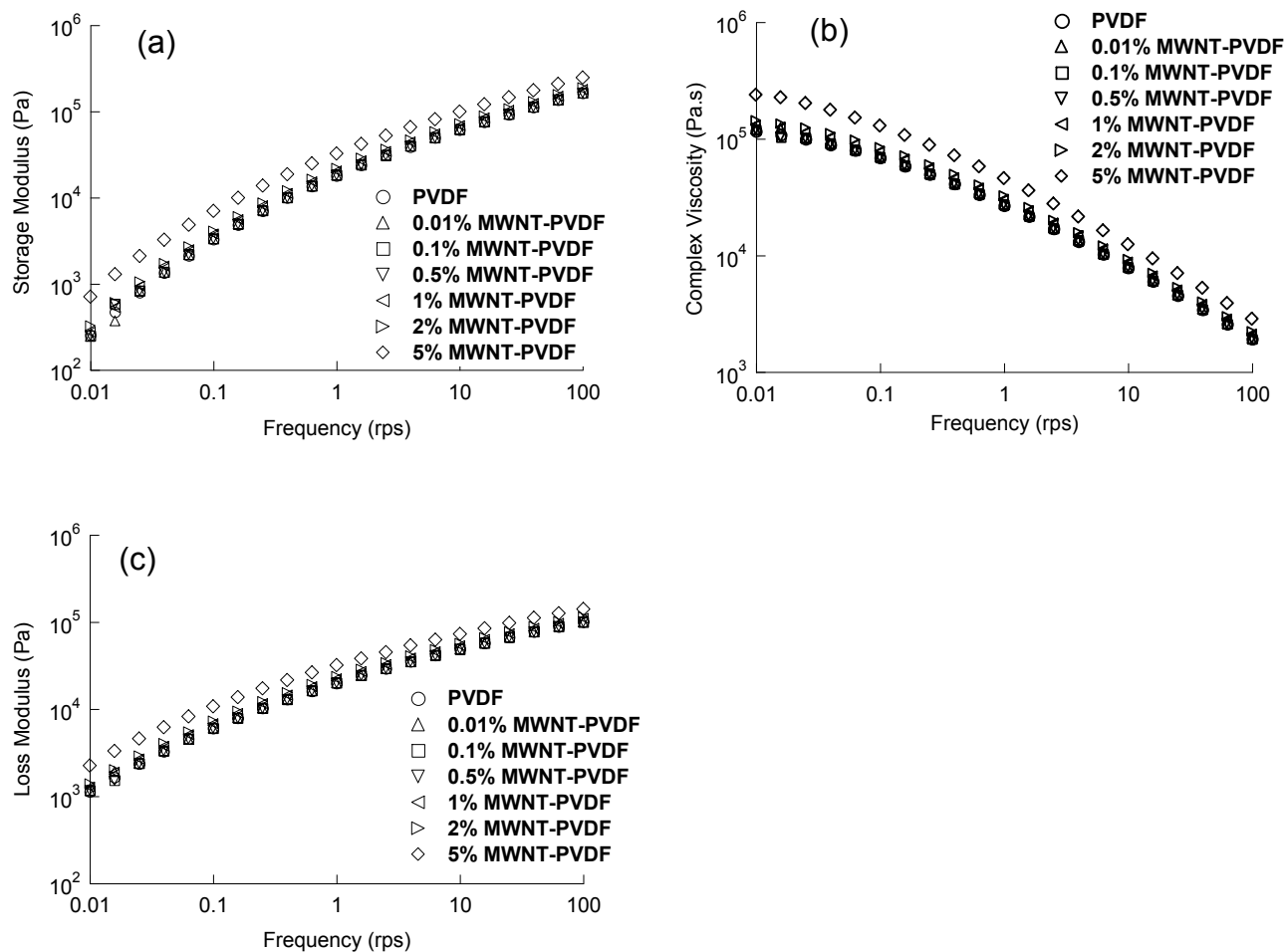


Figure 3: (a) Storage modulus, (b) Magnitude of complex viscosity, and (c) Loss modulus of PVDF nanocomposites at 190°C (1% strain)

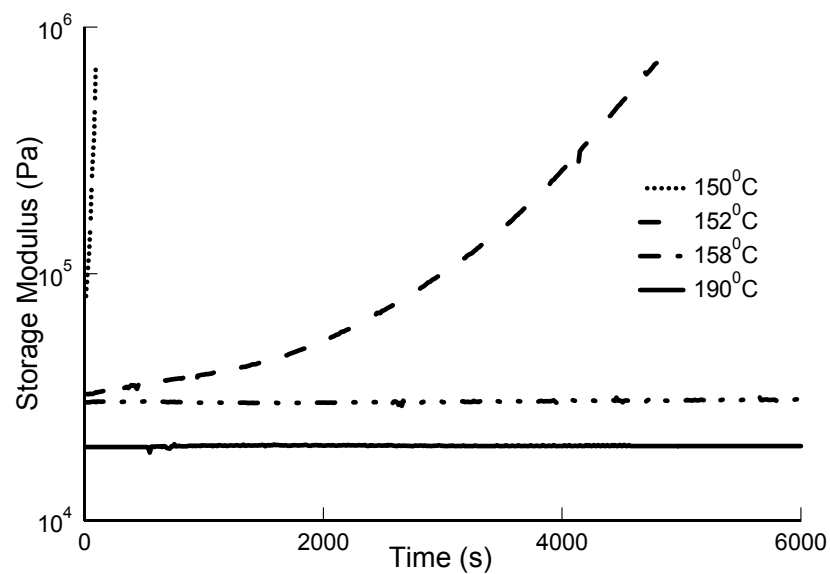


Figure 4: Change in storage modulus for pure PVDF sheared at different temperatures (1% strain, 1 rps)

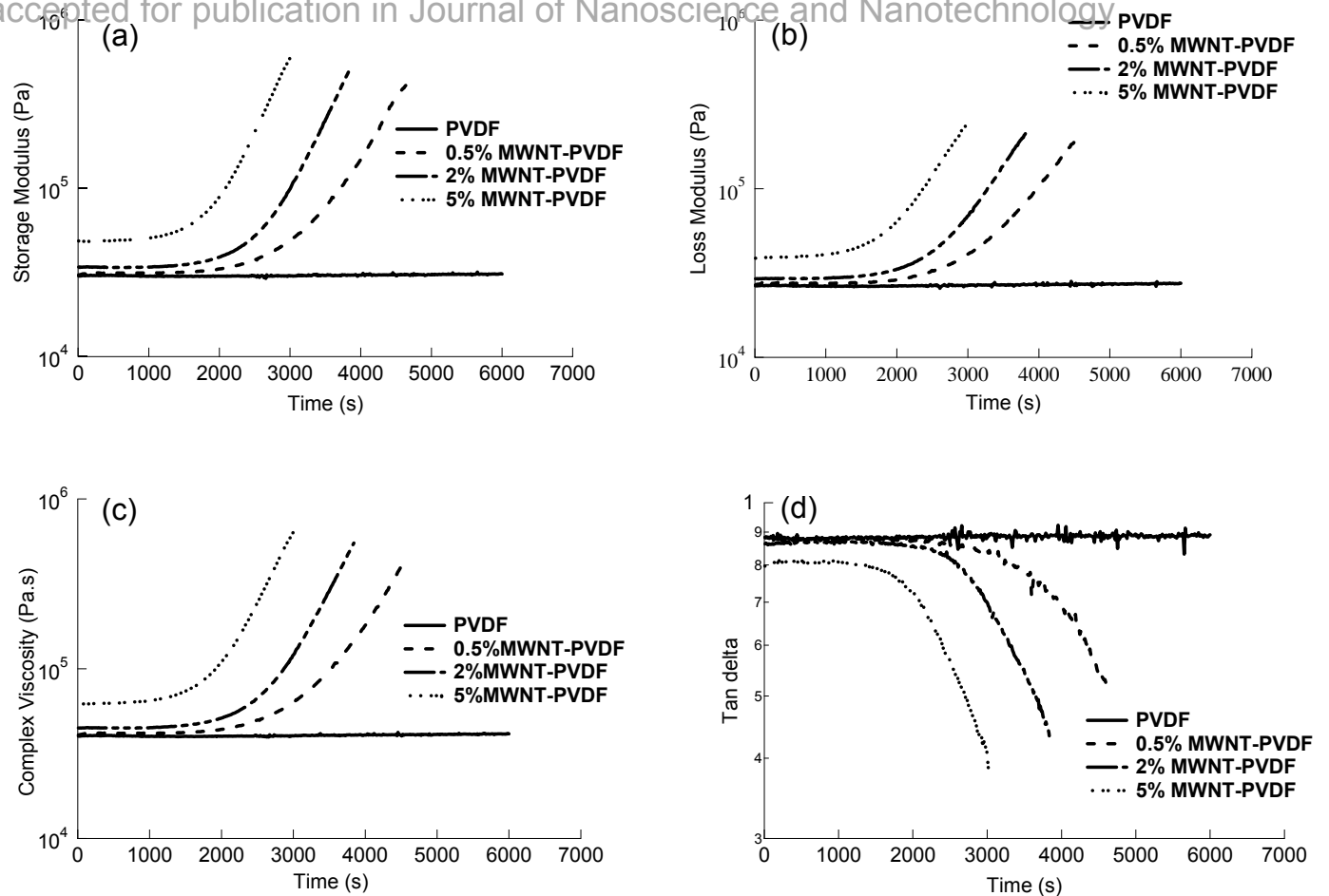


Figure 5: Variation of (a) Storage modulus, (b) Loss modulus, (c) Magnitude of complex viscosity and (d) Tan delta with time at 1% strain, 1 rps, at 158°C

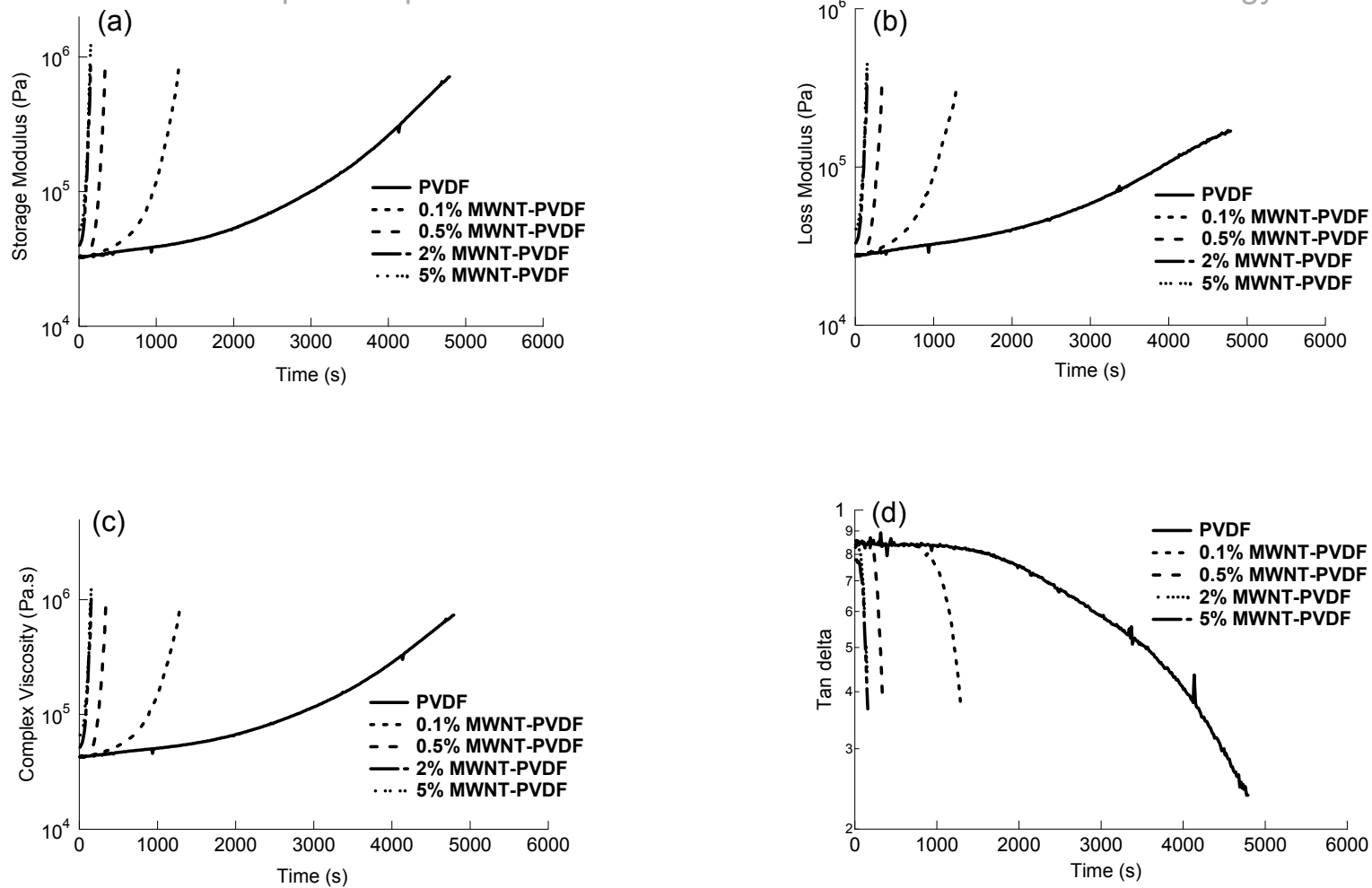


Figure 6: Variation of (a) Storage modulus, (b) Loss modulus, (c) Magnitude of complex viscosity and (d) Tan delta with time at 1% strain, 1 rps, at 152°C

Deformation induced crystallization and associated morphology development of carbon nanotube-PVDF nanocomposites, Mago, Fisher and Kalyon

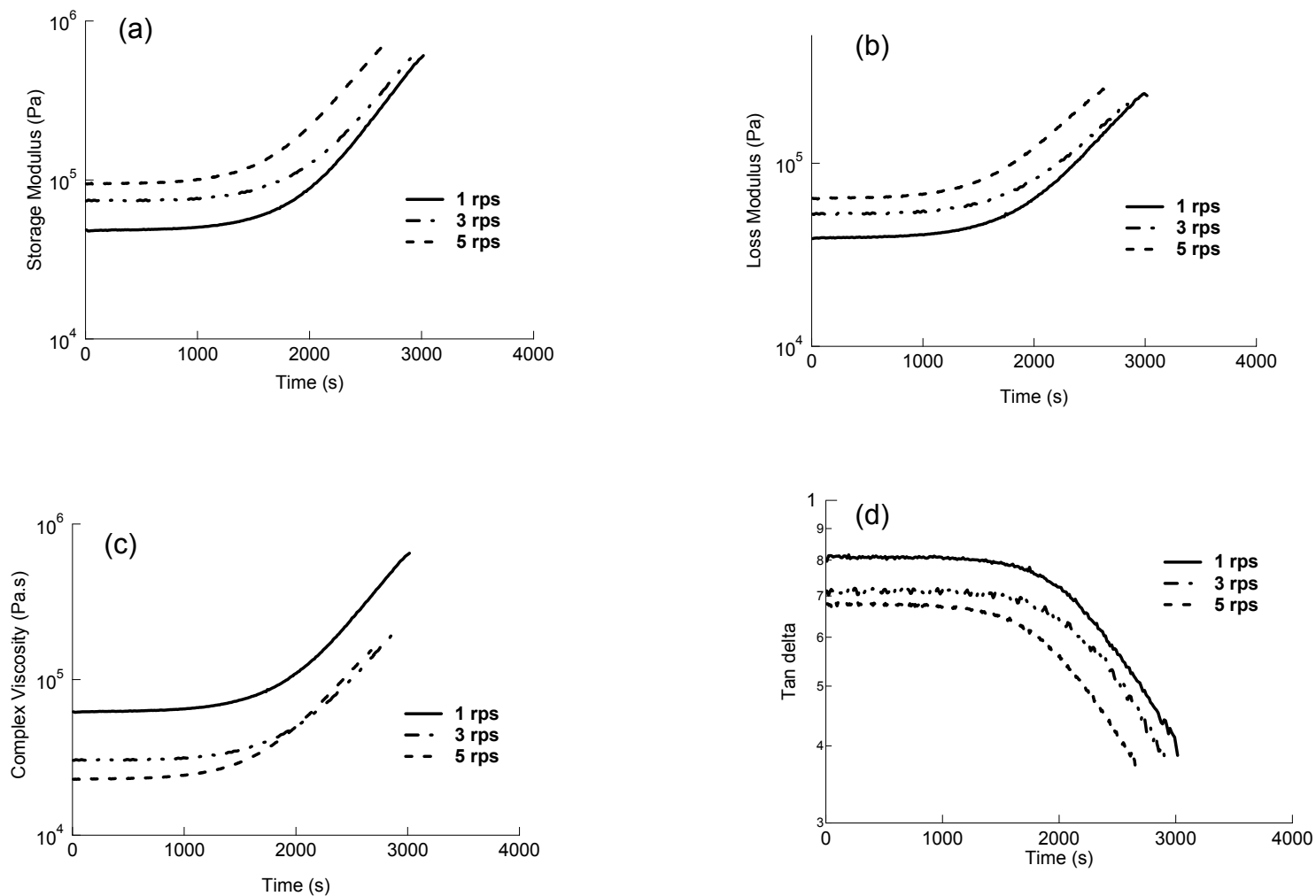


Figure 7: Variation of (a) Storage modulus, (b) Loss modulus, (c) Magnitude of complex viscosity and (d) Tan delta with increase in frequency, for 5%MWNT-PVDF nanocomposite at 1% strain, 158°C

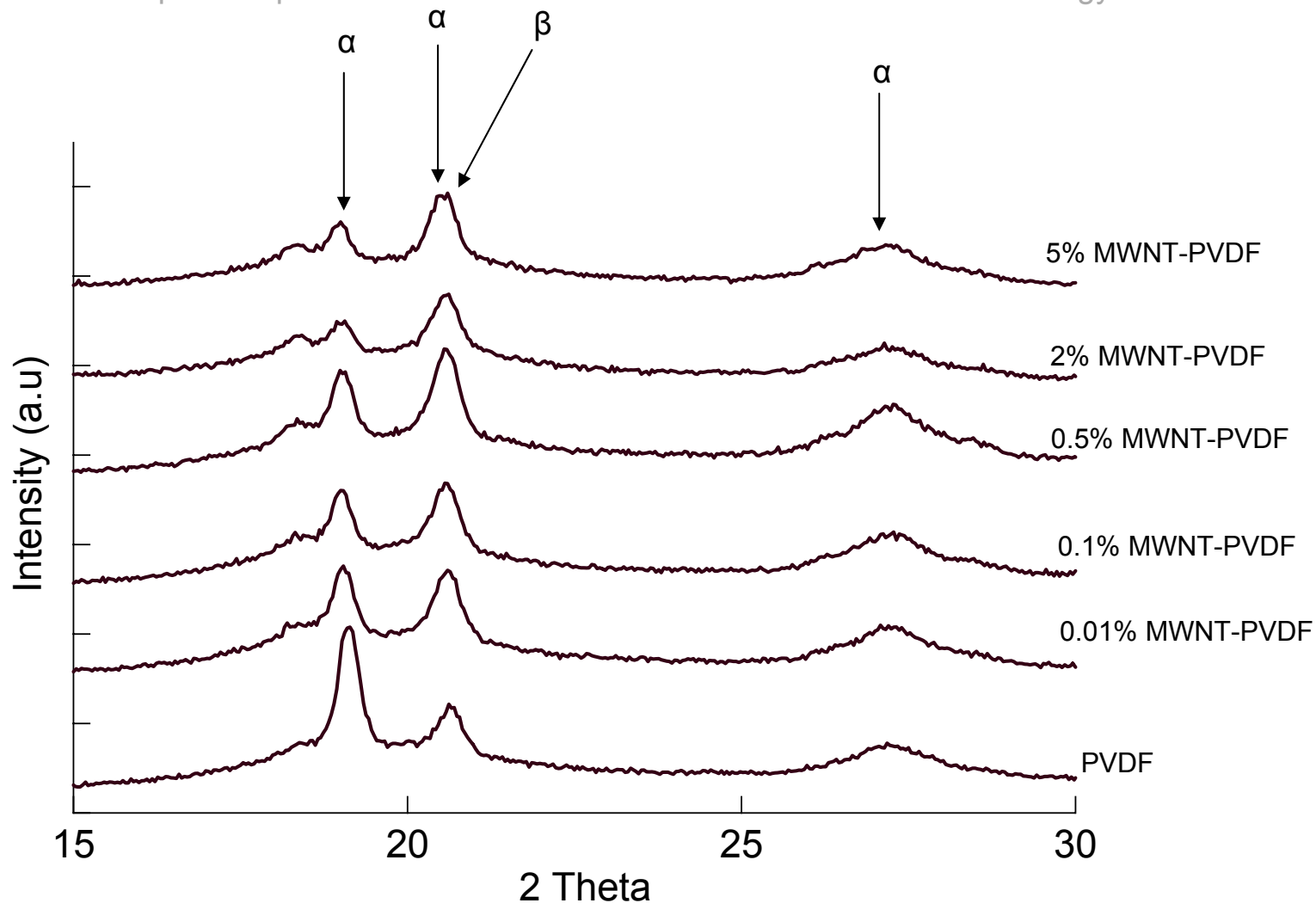


Figure 8: WAXD analysis of quiescent (compression molded) PVDF and PVDF nanocomposites

Deformation induced crystallization and associated morphology development of carbon nanotube-PVDF nanocomposites, Mago, Fisher and Kalyon

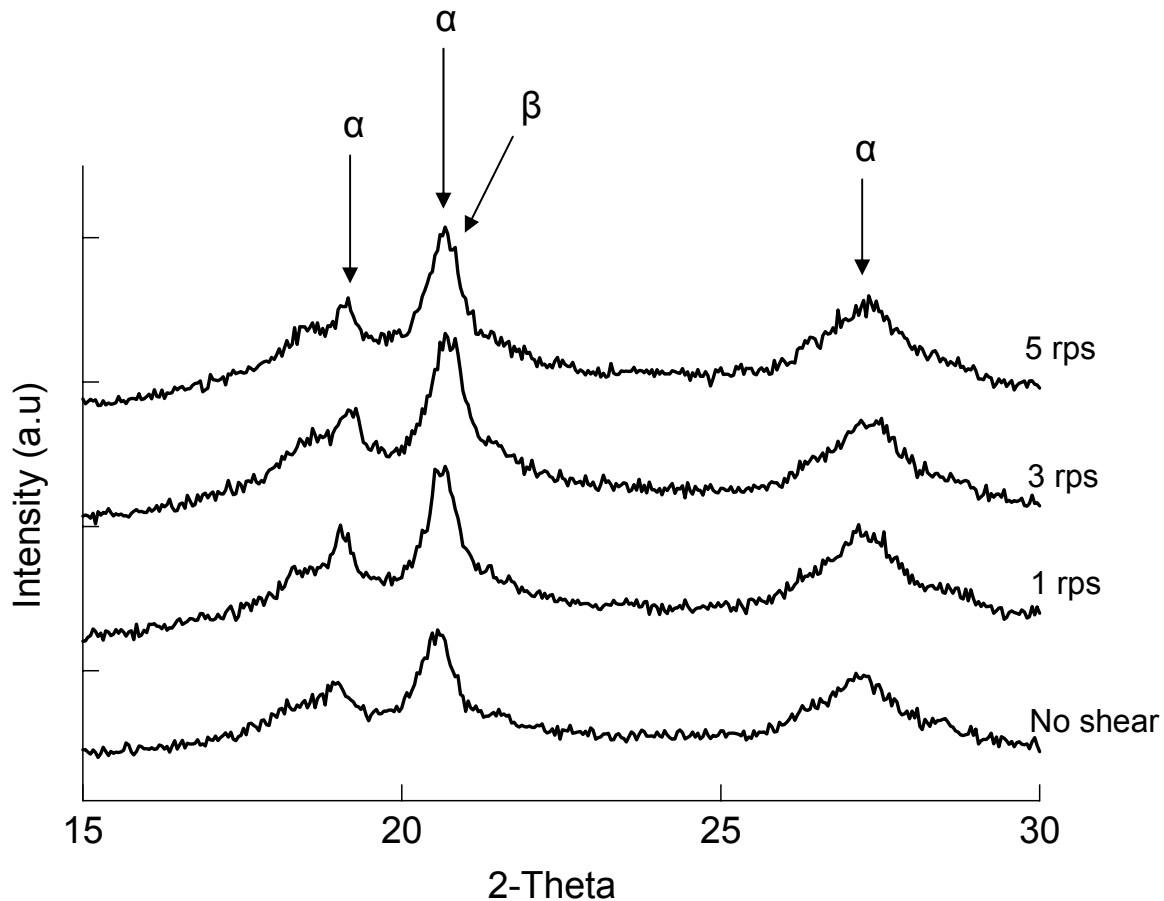


Figure 9: WAXD analysis of 5% MWNT-PVDF nanocomposites samples sheared at different frequencies (1% strain, 158°C)

Deformation induced crystallization and associated morphology development of carbon nanotube-PVDF nanocomposites, Mago, Fisher and Kalyon

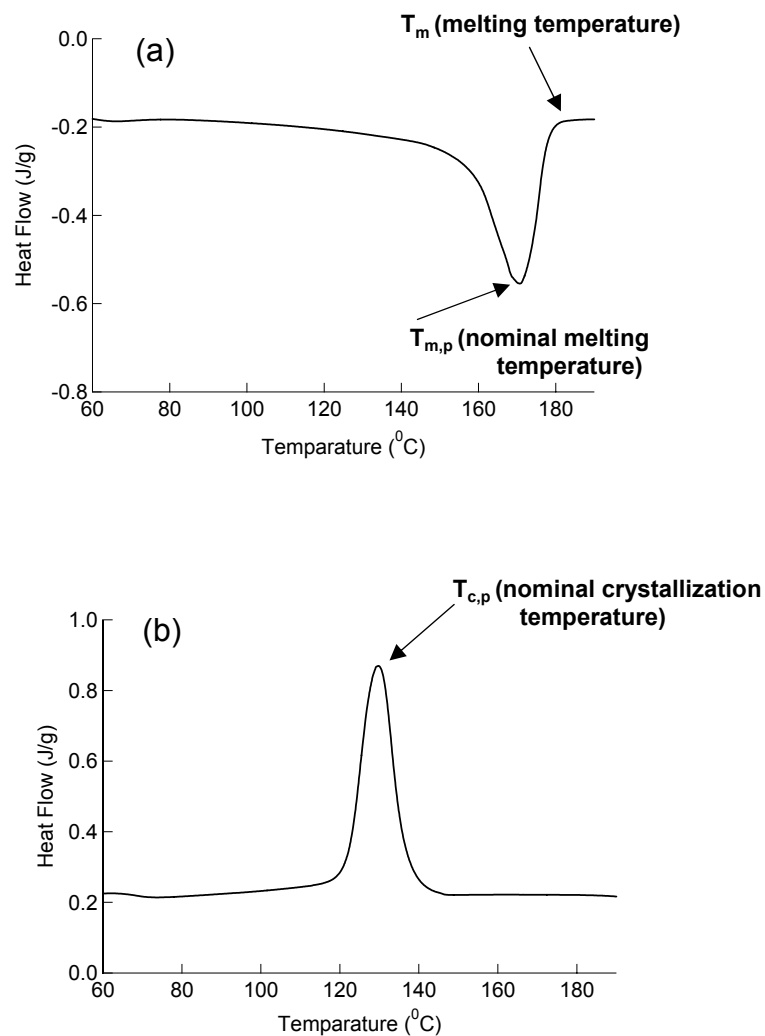


Figure 10: (a) Melting curve and (b) Non-isothermal crystallization curve for PVDF. Heating rate and cooling rate: 10°C/min

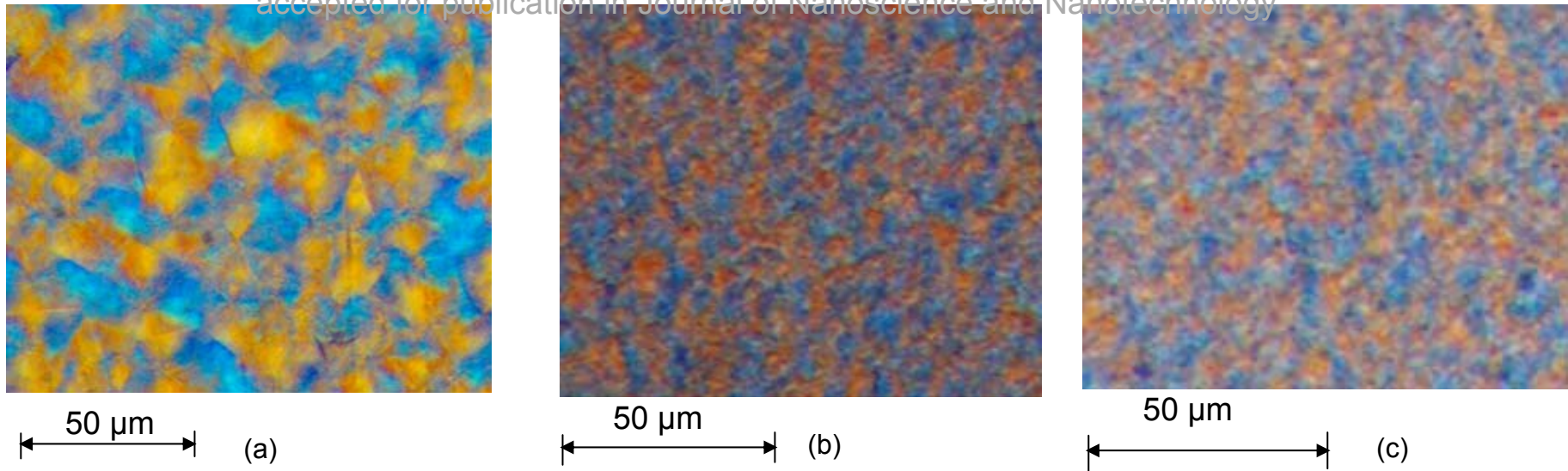


Figure 11: Effect of MWNT loading on PVDF crystal size: (a) Pure PVDF (b) 0.01%MWNT-PVDF (c) 0.1%MWNT-PVDF

Sample	$T_{m,p}$ (°C)	T_m (°C)	ΔH_m , J/g	X_c (%)	$T_{c,p}$ (°C)
PVDF	172.3 ± 1.7	182.3 ± 0.8	28 ± 2.0	26.8 ± 1.9	129.7 ± 0.8
0.01% MWNT – PVDF	171.1 ± 0.5	181.8 ± 0.4	29.5 ± 1.7	28.1 ± 1.6	137.2 ± 0.3
0.1% MWNT – PVDF	170.6 ± 1.4	180.5 ± 1.3	31 ± 1.3	29.6 ± 1.2	137.3 ± 0.1
0.5% MWNT – PVDF	170.3 ± 1.0	181.5 ± 0.3	30.5 ± 2.1	29.1 ± 2	140.2 ± 0.2
1% MWNT- PVDF	170.5 ± 0.5	181.4 ± 0.7	29.2 ± 2.5	27.9 ± 2.4	141.8 ± 0.1
2% MWNT- PVDF	170.8 ± 0.2	181.8 ± 0.8	30.5 ± 2.3	29.1 ± 2.1	142.6 ± 0.2
5% MWNT- PVDF	170.6 ± 0.3	181.3 ± 0.6	31.9 ± 2.7	30.5 ± 2.5	143.3 ± 0.1

Table 1. Nominal melting temperature ($T_{m,p}$), melting temperature (T_m), melting enthalpy (ΔH_m), crystallinity (X_c) and nominal crystallization temperature ($T_{c,p}$) of PVDF and PVDF nanocomposites under quiescent conditions. Heating rate and cooling rate: 10°C/min. The average values and 95% confidence intervals are reported (based on five separate tests per sample).

Frequency, rps	$T_{m,p}$ (°C)	T_m (°C)	ΔH_m , J/g	X_c (%)
No shear, in ARES for 3000s at 158°C	170.1 ± 0.7	180.4 ± 1.2	30.1 ± 3.3	28.8 ± 3.1
1	170.6 ± 2.0	180.6 ± 0.9	34.4 ± 2.2	32.9 ± 2.1
3	170.4 ± 1.5	181.6 ± 0.3	33.8 ± 0.7	32.3 ± 0.7
5	169.6 ± 0.1	182 ± 0.2	32.9 ± 2.2	31.5 ± 2.1

Table 2. Nominal melting temperature ($T_{m,p}$), melting temperature (T_m), melting enthalpy (ΔH_m) and crystallinity (X_c) of 5%MWNT- PVDF nanocomposites (sheared at 1% strain, 158°C). Heating rate: 10°C/min. The average values and 95% confidence intervals are reported (based on five separate tests per sample).